catalysts

MDPI

Article

Hard Template-Assisted Trans-Crystallization Synthesis of Hierarchically Porous Cu-SSZ-13 with Enhanced NH_3-SCR Performance

Fuzhen Yang, Ying Xin *, Xiaoli Zhu, Ahui Tang, Long Yu, Dongxu Han, Junxiu Jia, Yaning Lu and Zhaoliang Zhang

Shandong Provincial Key Laboratory of Fluorine Chemistry and Chemical Materials, School of Chemistry and Chemical Engineering, University of Jinan, Jinan 250022, China
* Correspondence: chm_xiny@ujn.edu.cn; Tel.: +86-531-8973-6032

Abstract: Small porous Cu-SSZ-13 catalysts have recently been commercialized for the selective catalytic reduction of NO_x with ammonia (NH_3-SCR) on diesel vehicles. Unfortunately, the conventional Cu-SSZ-13 catalyst still confronts the challenge of diffusion limitations, which represent a major obstacle that reduces the catalyst's SCR performance. Herein, a hierarchically porous SSZ-13 zeolite was synthesized via a trans-crystallization method assisted by the use of carbon black as a hard template in a short synthetic period, and the corresponding Cu-SSZ-13 catalysts with mesopores exhibited improved low-temperature activity and hydrothermal stability when compared with their microporous counterpart. A series of characterizations revealed that the mesopores are conducive to an increase in Cu loading while helping to stabilize the CHA structure and maintain the Cu species in their ionic form. More importantly, intra-particle diffusion limitations are reduced via the introduction of the mesopores owing to the shortened diffusion path inside the SSZ-13 zeolite, thus not only enhancing the active sites' accessibility but also promoting the diffusion of the reactants and products. This work contributes to the design and synthesis of a high-performance Cu-SSZ-13 zeolite SCR catalyst for the removal of NO_x emitted from diesel vehicles.

Keywords: Cu-SSZ-13; hierarchically porous; NH_3-SCR; trans-crystallization; hard template

check for updates

Citation: Yang, F.; Xin, Y.; Zhu, X.; Tang, A.; Yu, L.; Han, D.; Jia, J.; Lu, Y.; Zhang, Z. Hard Template-Assisted Trans-Crystallization Synthesis of Hierarchically Porous Cu-SSZ-13 with Enhanced NH_3-SCR Performance. *Catalysts* **2023**, *13*, 1217. https://doi.org/10.3390/catal13081217

Academic Editor: Ioannis V. Yentekakis

Received: 30 June 2023
Revised: 31 July 2023
Accepted: 7 August 2023
Published: 16 August 2023

1. Introduction

Nitrogen oxides (NO_x) emitted from the combustion of fossil fuels are major gaseous pollutants which contribute to a number of environmental pollution issues and are harmful to human health [1]. Nowadays, with an increasing number of diesel engines due to their high power and fuel economy, diesel exhaust is the primary source of NO_x emissions [2,3]. To comply with current and future emission regulations, it is urgent and imperative to eliminate NO_x emissions from diesel engines. Among the various NO_x removal technologies, the selective catalytic reduction of NO_x with ammonia (NH_3-SCR) is regarded as the most efficient method [4,5], and copper (Cu)-exchanged SSZ-13 zeolites are now commercial products for NH_3-SCR catalysts due to their outperformance in reducing diesel engine NO_x emissions compared with traditional vanadia-based (V_2O_5-WO_3/TiO_2) catalysts [6–10]. However, the SSZ-13 zeolite has a chabazite (CHA) structure with a relatively small pore radius of 3.8 Å in an eight-membered ring, which may limit the mass transfer of reactants in channels [11,12]. In addition, the intra-particle diffusion limitation has been found to be the dominating limitation factor and plays a key role in the performance of NH_3-SCR in Cu-SSZ-13 catalysts [13]. In order to overcome the diffusion limitation, hierarchical pores are introduced into the SSZ-13 zeolite, and the presence of mesopores can enhance mass transport and reduce the residence time of molecules in the micropores by shortening their diffusion length [14]. Both the catalytic activity and lifetimes of zeolite catalysts can be significantly improved via the hierarchically porous structure [15].

Generally, two approaches have been effectively employed to fabricate hierarchical pores in SSZ-13 zeolites. One approach is to use a postsynthetic modification, such as dealumination and desilication, in which the zeolites are treated via steaming at a high temperature or leaching with acidic/alkaline solutions [16–18]. Although some of these methods are economical and can be feasibly scaled up, they are usually environmentally unfriendly, and the structural and physicochemical properties of the final zeolite can not be accurately controlled [19–21]. The alternative bottom-up strategy is the in situ synthesis method in which hierarchical pores are created by employing soft or hard templates during the hydrothermal synthesis procedure [17]. Initially, Wu et al., developed a dual-template method to directly synthesize mesoporous SSZ-13 zeolites via the use of trimethyl-adamantanammonium hydroxide (TMAdaOH) and a diquaternary ammonium mesoporogen; consequently, the high level of interconnectivity of the micro- and mesopores within the SSZ-13 zeolite delivered an improved stability of it as an acid catalyst in the methanol-to-olefins (MTO) reaction [22]. Thereafter, the introduction of mesoporosity into SSZ-13 zeolites was proved to improve their catalytic performance in MTO reactions via the partial substitution of TMAdaOH with $C_{16}H_{33}$-[N^+-methylpiperidine] [23]. Furthermore, Liu et al. employed the same method to fabricate a hierarchical Cu-SSZ-13 catalyst with controllable pores in which the synergistic effect of the micropores and mesopores improved the adsorption of NO and NH_3, and thus the SCR activity [24]. Meanwhile, hierarchically porous Cu-SSZ-13 catalysts also exhibited an improved SO_2 tolerance because the existence of the mesopores alleviated the accumulation of sulfates [25]. In addition to soft templates, hard templates (e.g., inorganic materials, carbonaceous materials, biological materials, and polymers) have been successfully used for the preparation of hierarchically porous zeolites; in particular, carbonaceous materials have been widely used due to their chemical inertness, structural diversity, cost-effectiveness, and ease of removal together with templates via calcination [26,27]. Accordingly, hierarchically porous Cu-SSZ-13 was prepared by adopting carbon black as a hard template [28]. The obtained Cu-SSZ-13 catalyst with ordered mesopores exhibited superior low-temperature activity, hydrothermal stability, and poisoning resistance when compared with a Cu-SSZ-13 catalyst without mesopores. However, the preparation method was based on the traditional hydrothermal synthesis method; therefore, the crystallization process required a long time (at least three days), indicating a low level of efficiency and high energy consumption. Therefore, it is critical and urgent to build a simple, scalable, and cost-effective strategy to synthesize hierarchically porous Cu-SSZ-13 catalysts that demonstrate enhanced SCR performance in NO_x removal.

In view of the above-mentioned facts, a robust interzeolite transformation strategy was reported in which a coke-containing spent ZSM-5 zeolite was used as the raw material and a hierarchical SSZ-13 zeolite was fabricated by combining a hard template (the coke confined in the spent ZSM-5) with a trans-crystallization process [29]. Moreover, the trans-crystallization of the CHA zeolite via the FAU zeolite demonstrated a higher level of efficiency and more environmental benefits than synthesizing a zeolite using an aluminosilicate gel in the conventional hydrothermal method because the decomposition/dissolution of an FAU zeolite gives rise to locally ordered aluminosilicate species that assemble and evolve into a CHA zeolite [30,31]. Inspired by these studies, we developed a hard template-assisted trans-crystallization method to synthesize a hierarchically porous SSZ-13 zeolite in a short synthetic period. In this method, carbon black, TMAdaOH, and a FAU zeolite were used as the mesoporogen, structure-directing agent (SDA), and raw material, respectively. A schematic diagram of the synthesis procedure is shown in Figure 1. Following an ion exchange process with Cu^{2+} ions, the obtained hierarchically porous Cu-SSZ-13 catalysts exhibit enhanced low-temperature activity and hydrothermal stability compared with their microporous counterpart in NH_3-SCR reactions due to the reduction in the intra-particle diffusion limitation via the introduction of mesopores. This work provides not only a simple and efficient way to synthesize hierarchically porous zeolites but also a guideline to design and prepare the high-performance SCR catalyst in NO_x removal.

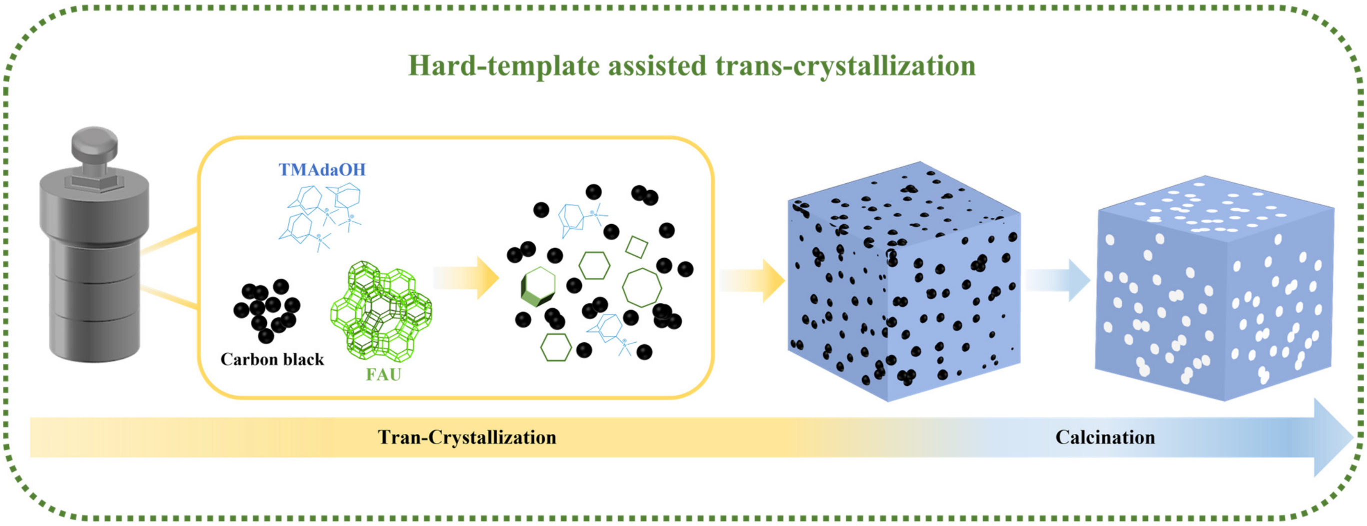

Figure 1. The schematic diagram of synthetic procedure for hierarchically porous SSZ-13 zeolite.

2. Results and Discussion

The hierarchically porous SSZ-13 zeolites were synthesized via the trans-crystallization of FAU zeolite with carbon black as a hard template, which are denoted as SSZ-13-*x* hereafter (*x* represents the molar composition of carbon black in the initial mixture before crystallization). To further clarify the contribution of mesopores in SSZ-13 zeolites to the SCR performance, the hierarchically porous Cu-SSZ-13 catalysts were then prepared via ion-exchange treatment (denoted as Cu-SSZ-13-*x*), and the aged catalysts were obtained by hydrothermal aging at 800 °C for 16 h (denoted as Cu-SSZ-13-*x*-800) in order to assess their hydrothermal stability.

2.1. Structural and Morphological Characterizations of SSZ-13-x Zeolites

The X-ray diffraction (XRD) patterns of the obtained SSZ-13-*x* zeolites are shown in Figure 2. The diffraction peaks of SSZ-13-*x* zeolites are consistent with those of SSZ-13 reported in a previous work [32], indicating the negligible changes in CHA structure with the introduction of carbon black during trans-crystallization processes to fabricate mesopores. Notably, the two peaks at around 30–32° can be clearly divided in the XRD pattern of SSZ-13-0, while those of the SSZ-*x* (x = 0.33, 0.55, 0.77) samples seem to overlap. This distinction is generated from the hierarchical structure of the zeolites. It is possible that the introduction of mesopores affected the spatial arrangement of the micropores to a certain extent, slightly changing the position and intensity of XRD peaks.

To check whether or not the mesopores exist in the obtained SSZ-13-*x* zeolites, N_2 adsorption/desorption measurements and scanning electron microscope (SEM) observations were performed, and the results are shown in Figures 3 and 4, respectively. N_2 adsorption/desorption isotherms of SSZ-13-*x* zeolites reveal that SSZ-13-0 displays the type I isotherms (Figure 3a), with no obvious hysteresis loop, indicating the typical microporosity [33]. The hierarchically porous SSZ-13-*x* (x = 0.33, 0.55, and 0.77) zeolites present typical type I+IV isotherms with a clear H4 hysteresis loop at a relative pressure at $P/P_0 > 0.5$, which are attributed to the existence of mesopores in a broad pore-size distribution of 5–20 nm (Figure 3b). The surface areas and pore volumes of the zeolites are summarized in Table 1. The pore volumes of the hierarchically porous zeolites are obviously higher than that of SSZ-13-0, which could be ascribed to the existence of mesopores. However, there is a slight difference in specific surface areas of the zeolites.

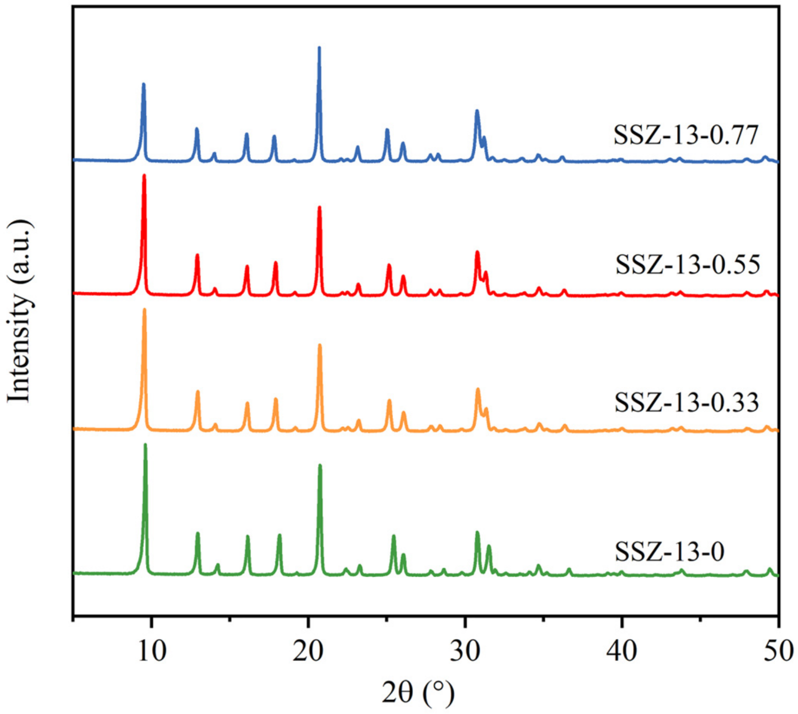

Figure 2. XRD patterns of SSZ-13-*x* zeolites.

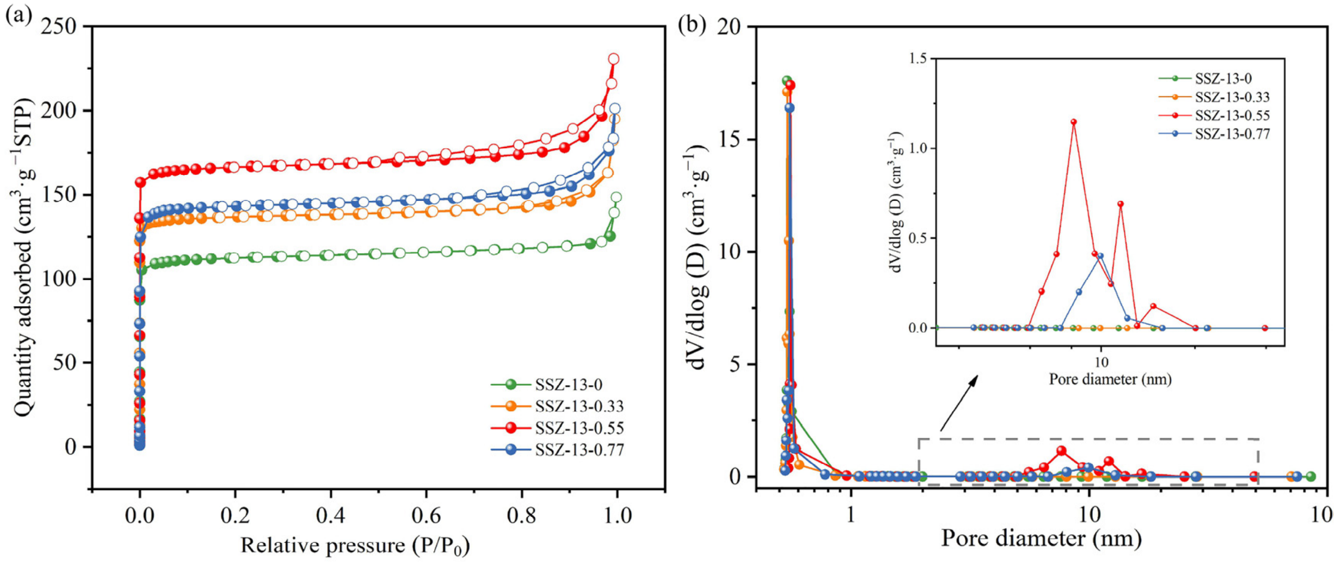

Figure 3. (**a**) N_2 adsorption/desorption isotherms and (**b**) pore size distribution curves of SSZ-13-*x* zeolites.

Table 1. Textural properties and quantitative analysis of SSZ-13-*x* zeolites by N_2 adsorption/desorption and SEM characterizations.

Sample	Surface Areas ($m^2 \cdot g^{-1}$)	Pore Volume ($cm^3 \cdot g^{-1}$)	Si/Al Ratio [a]	Average Grain Size [a] (nm)
SSZ-13-0	590.0	0.23	5.6	910
SSZ-13-0.33	561.5	0.30	6.0	520
SSZ-13-0.55	608.9	0.37	6.1	470
SSZ-13-0.77	575.2	0.35	6.4	419

[a] Derived from SEM observations and EDS mappings.

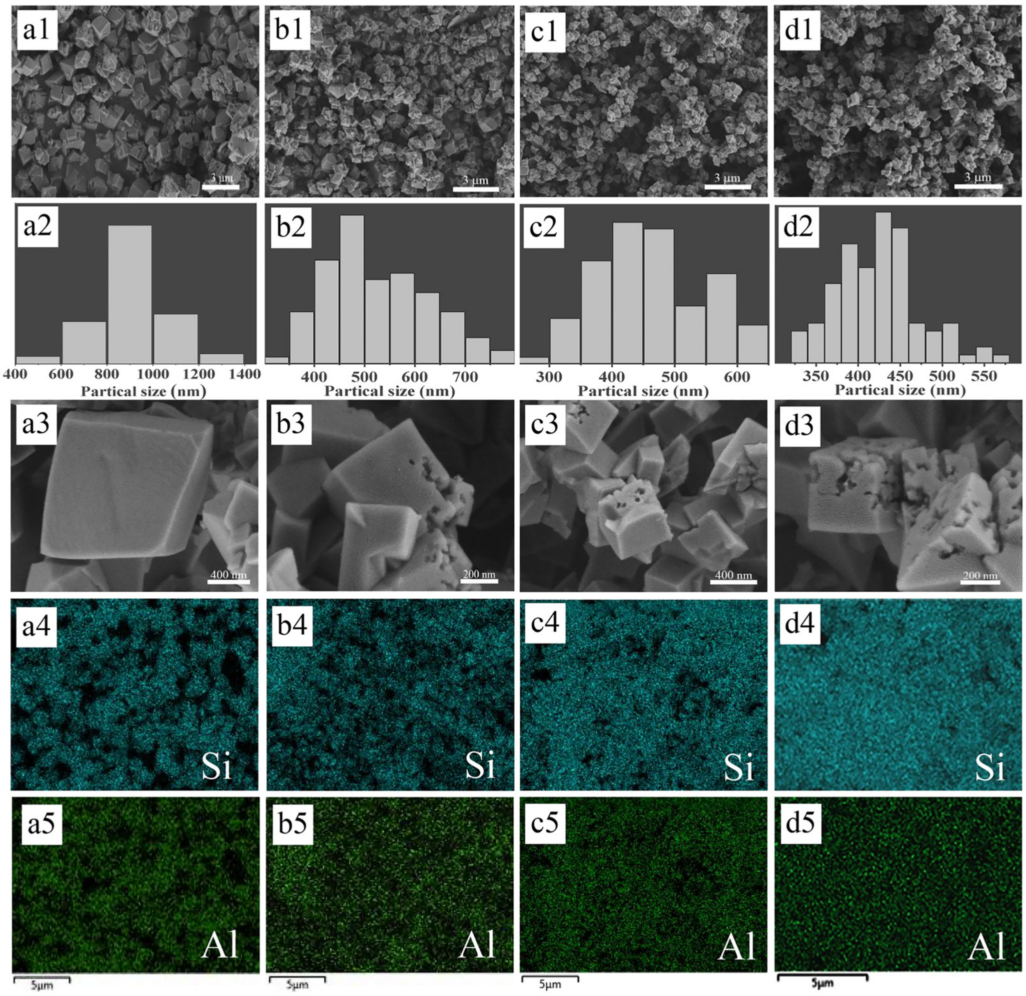

Figure 4. SEM images and EDS mappings of SSZ-13-*x* zeolites: (**a**) SSZ-13-0, (**b**) SSZ-13-0.33, (**c**) SSZ-13-0.55, and (**d**) SSZ-13-0.77. (**1**,**3**) SEM images, (**2**) particle size distribution, (**4**) distribution of Si element, and (**5**) distribution of Al element.

As shown in SEM images of the obtained SSZ-13-*x* zeolites (Figure 4), SSZ-13-0 exhibits typical cubic crystals with a primary particle size of about 910 nm (Figure 4(a1,a2), and Table 1). When carbon black was used as a hard template, the zeolite precursors nucleate on the outside of carbon black and grow in a continuous mode, encapsulating the carbon black. After calcination, mesopores are generated from the spaces initially occupied by the carbon black. In addition, a large amount of carbon black could increase the concentration of crystal nuclei, resulting in the reduction in the zeolite crystal size [26]. Consequently, the grain sizes of the zeolites are gradually decreased from 520 nm to 419 nm via increasing the additive amounts of carbon black (Figure 4(b1–d1,b2–d2)), indicating that the amounts of carbon black have a positive effect on reducing the grain sizes. Notably, a number of pores and slits in various sizes are clearly perceived in the zeolite particles (Figure 4(b3–d3)), confirming the mesopores are introduced into the crystallites of SSZ-13-*x* (*x* = 0.33, 0.55, and 0.77). EDS mapping was conducted in conjunction with SEM observations to probe the element distributions within the SSZ-13-*x* zeolites (Figure 4(a4–d4,a5–d5)). The Si and Al mappings display uniform distributions in all the samples without exhibiting distinct enrichment in any hierarchically porous ones. Moreover, the Si/Al ratios of SSZ-13-*x* zeolites were quantified according to EDS mappings, and the results are listed in Table 1. The Si/Al ratio of SSZ-13-*x* (*x* = 0.33, 0.55, and 0.77) is slightly higher than that of SSZ-13-0, which is conducive to the skeleton stability of the hierarchically porous zeolites. The above results confirm that the carbon black-assisted trans-crystallization method leads to the successful synthesis of the hierarchically porous SSZ-13 zeolites.

2.2. SCR Performance of Cu-SSZ-13-x Catalysts

As shown in Figures 5a and S1a, all the catalysts exhibit over 90% NO_x conversion and high N_2 selectivity from 200 to 600 °C. As expected, the hierarchically porous Cu-SSZ-13-*x* catalysts showed higher NO_x conversion at low temperatures than Cu-SSZ-13-0. Notably, the NO_x conversion of Cu-SSZ-13-0.55 reaches 92% at 175 °C, increasing by 20% compared with that of Cu-SSZ-13-0. According to the previous literature [34], the enhanced low-temperature activity of Cu-SSZ-13-*x* catalysts could be ascribed to their higher surface area together with the coexistence of micropores and mesopores, which promote the diffusion of the reactants and products. To better demonstrate the difference between catalysts, the SCR activity of the catalysts was measured at a higher gas hourly space velocity (GHSV) of 800,000 h^{-1} (Figure S2). It is evident that the NO_x conversions decrease markedly at a high GHSV, and the intrinsic activity of Cu-SSZ-13-*x* (x = 0.33, 0.55, and 0.77) are higher than that of Cu-SSZ-13-0, indicating that the diffusion limitation still exists in the Cu-SSZ-13 catalyst without mesopores [31]. Unfortunately, no significant difference was observed among Cu-SSZ-13-*x* catalysts with mesopores, probably due to the contents of the mesopore having no impact on the intrinsic activity of the catalysts. After hydrothermal aging, the SCR activity of all the catalysts distinctly decreased across the entire temperature range, particularly for Cu-SSZ-13-0, in which the NO_x conversion fell to ca. 40% at 200 °C and exhibited a narrow active temperature window (NO_x conversion > 90%) at 300–400 °C (Figures 5b and S1b). In contrast, Cu-SSZ-13-*x* catalysts maintained excellent SCR activity with the NO_x conversions exceeded 90% from 250 to 500 °C. Especially for Cu-SSZ-13-0.55, the NO_x conversions reached more than 80% up to 600 °C. These results indicate that the introduction of mesopores effectively alleviates the decrease in SCR activity and hydrothermal aging deactivation of the Cu-SSZ-13 catalyst. It is speculated that mesopores might provide the interspaces to hinder the migration and aggregation of CuO_x species segregated from the Cu-SSZ-13 catalyst during hydrothermal aging, and thus guarantee a wide active temperature window and structural stability.

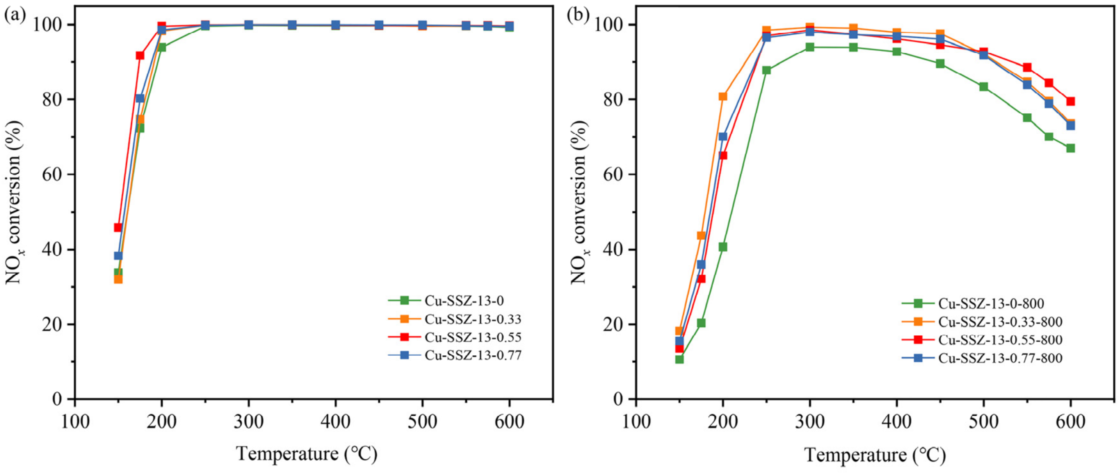

Figure 5. NO_x conversion of (**a**) Cu-SSZ-13-*x* and (**b**) Cu-SSZZ-13-*x*-800 catalysts at a gas hourly space velocity of 400,000 h^{-1}.

In order to clarify how the mesopores enhance the SCR performance of the Cu-SSZ-13 catalyst, Cu-SSZ-13-0.55 with superior low-temperature activity and hydrothermal stability was chosen to be comprehensively characterized as below. The microporous counterpart, Cu-SSZ-13-0, was also studied as a reference.

2.3. Characterizations of Cu-SSZ-13-0.55 and Cu-SSZ-13-0 Catalysts

As can be seen from Figure 6, both Cu-SSZ-13-0 and Cu-SSZ-13-0.55 exhibit the CHA structure after Cu ion-exchange, and no diffraction peaks of CuO_x species are observed, indicating that the Cu species are highly dispersed in the zeolites. Importantly, both Cu-

SSZ-13-0-800 and Cu-SSZ-13-0.55-800 catalysts maintain the CHA structure without CuO_x species even after hydrothermal aging. The surface area and pore volume of Cu-SSZ-13-0 and Cu-SSZ-13-0.55 are slightly decreased in comparison with SSZ-13-*x* zeolites due to the Cu loading (Table 2 and Figure S3). The further decrease in surface areas for Cu-SSZ-13-0-800 and Cu-SSZ-13-0.55-800 indicate that the hydrothermal aging treatment has threatened the porous structure of the catalysts to a certain extent, leading to the decrease in NO_x conversions (Figure 5).

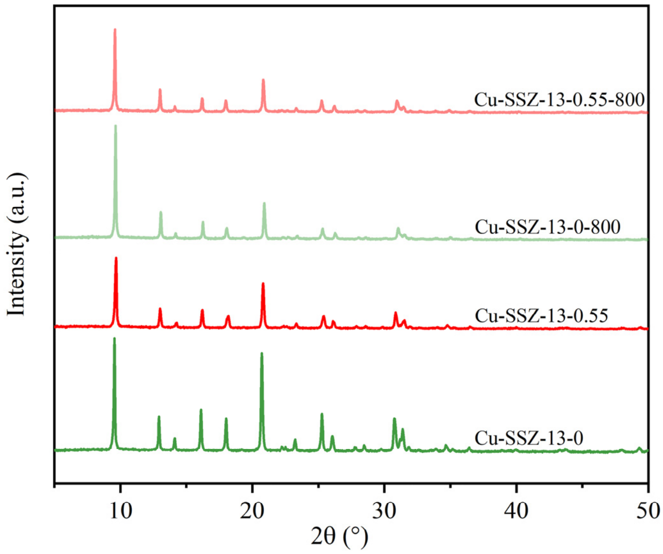

Figure 6. XRD patterns of Cu-SSZ-13-0 and Cu-SSZ-13-0.55 catalysts before and after hydrothermal aging.

Table 2. Textural properties and quantitative analysis of Cu-SSZ-13-0 and Cu-SSZ-13-0.55 catalysts before and after hydrothermal aging.

Sample	**Surface Areas ($m^2 \cdot g^{-1}$)**	**Pore Volume ($cm^3 \cdot g^{-1}$)**	**Si/Al Ratio [a]**	**Cu Loading [a] (wt.%)**	**Average Grain Size [a] (nm)**
Cu-SSZ-13-0	586.3	0.26	5.3	3.8	961
Cu-SSZ-13-0.55	607.2	0.29	6.1	4.1	449
Cu-SSZ-13-0-800	559.4	0.26	5.7	3.9	591
Cu-SSZ-13-0.55-800	564.4	0.27	6.0	4.2	470

[a] Derived from SEM observations and EDS mappings.

The morphology of Cu-SSZ-13-*x* catalysts was also investigated by SEM observations. Cu-SSZ-13-0 exhibits typical cubic crystals with a primary particle size of about 961 nm (Figure 7(a1–a3), and Table 2), while the cubic grain size of Cu-SSZ-13-0.55 reduces to 449 nm (Figure 7(b1,b2), and Table 2). The smaller grain size of Cu-SSZ-13-0.55 may contribute to the enhanced low-temperature activity due to a shorter diffusion path that promotes the diffusion of reactants and products to the outer surface of catalysts, thereby reducing the intra-particle diffusion limitation. After hydrothermal aging, the grain size is further reduced, and that of Cu-SSZ-13-0-800 drops to 591 nm (Figure 7(c1–c3), and Table 2), suggesting the hydrothermal aging results in the collapse of the framework in Cu-SSZ-13-0. On the contrary, the grain size of Cu-SSZ-13-0.55-800 is negligibly changed (Figure 7(d1,d2), and Table 2), indicating that promoted hydrothermal stability is probably derived from the introduction of mesopores. Moreover, the nanoscaled pores and slits remain unchanged before and after hydrothermal aging (Figure 7(b3,d3)), which not only enhances the active sites' accessibility but also promotes the diffusion of the reactants and products.

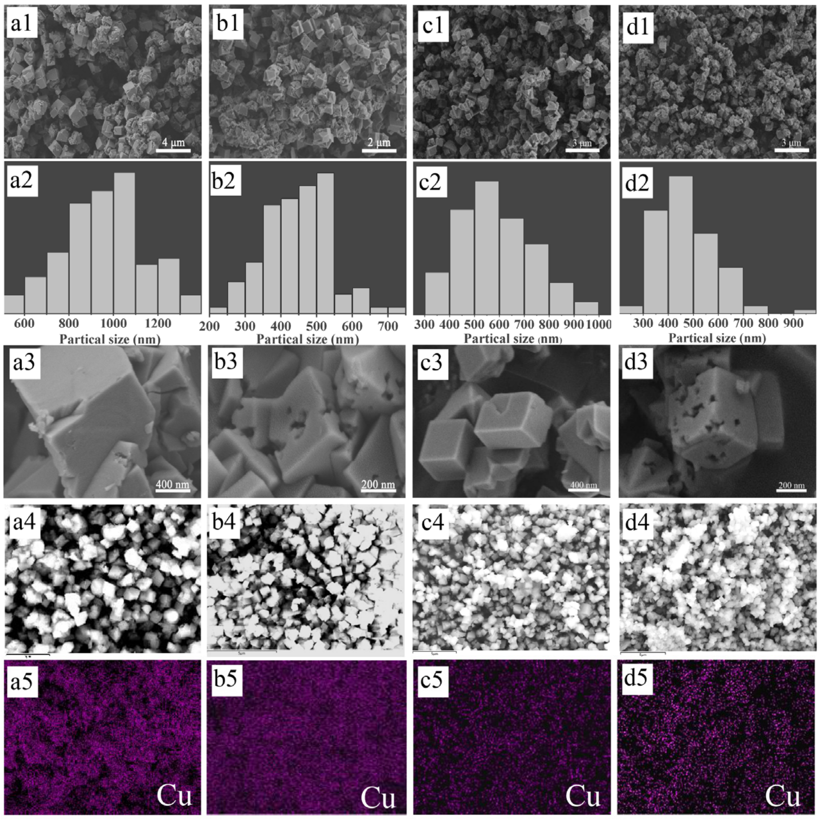

Figure 7. SEM images and EDS mappings of the catalysts: (**a**) Cu-SSZ-13-0, (**b**) Cu-SSZ-13-0.55, (**c**) Cu-SSZ-13-0-800, and (**d**) Cu-SSZ-13-0.55-800. (**1**,**3**,**4**) SEM images, (**2**) particle size distribution, and (**5**) distribution of Cu element.

EDS mapping was performed to examine the element distributions of the catalysts (Figures 7(a4–d4,a5–d5) and S4). As shown in Figure 7(a5–d5), the Cu mappings display good distributions in all samples, and no distinct enrichment of the Cu element is observed in the hydrothermally aged ones. The quantified Si/Al ratios and Cu loadings are listed in Table 2. It is observed that the Si/Al ratio of Cu-SSZ-13-0.55 is still slightly higher than that of Cu-SSZ-13-0, accounting for its higher hydrothermal stability. Meanwhile, the Cu loadings are also increased in Cu-SSZ-13-0.55, which can be attributed to the enhanced diffusion efficiency of Cu species into the zeolite during the ion-exchange procedure. All of the above factors contribute to improving the SCR performance of Cu-SSZ-13 catalysts, particularly in terms of the low-temperature activity and hydrothermal stability [35].

Actually, although EDS mappings results display negligible changes in the composition of catalysts before and after hydrothermal aging, the Si and Al arrangements in zeolites experience a significant variation during the hydrothermal aging process. To detect the local environment of Si and Al in the catalysts, ^{29}Si magic angle spin nuclear magnetic resonance (^{29}Si MAS NMR) and ^{27}Al MAS NMR spectra were measured. As shown in Figure 8a, ^{29}Si MAS NMR spectra of the catalysts exhibit three framework tetrahedral Si (Q^4) features at −111, −105, and −99 ppm, corresponding to the tetrahedral Si coordinated with four Si neighbors (defined as Q^4(0Al), Si(OSi)$_4$), the tetrahedral Si coordinated with three Si and one Al neighbors (defined as Q^4(1Al), Si(OSi)$_3$(OAl)), and the tetrahedral Si coordinated with two Si and two Al neighbors (defined as Q^4(2Al), Si(OSi)$_2$(OAl)$_2$), respectively [36–38]. To analyze the evolution of Si species before and after hydrothermal aging, the proportions of different Si species as well as the Si/Al ratios of zeolite framework are estimated by deconvolution of ^{29}Si MAS NMR spectra (Table 3). Obviously, the framework Si/Al ratios of both Cu-SSZ-13-0 and Cu-SSZ-13-0.55 are similar to those derived from the EDS mappings. In contrast, they are significantly increased after hydrothermal aging, which could be attributed to the dealumination of the zeolite framework caused by hydrothermal aging. Interestingly, Cu-SSZ-13-0.55 exhibits a slightly lower increase compared to Cu-SSZ-13-0, indicating its higher hydrothermal stability, which matches with the SCR performance (Figure 5b).

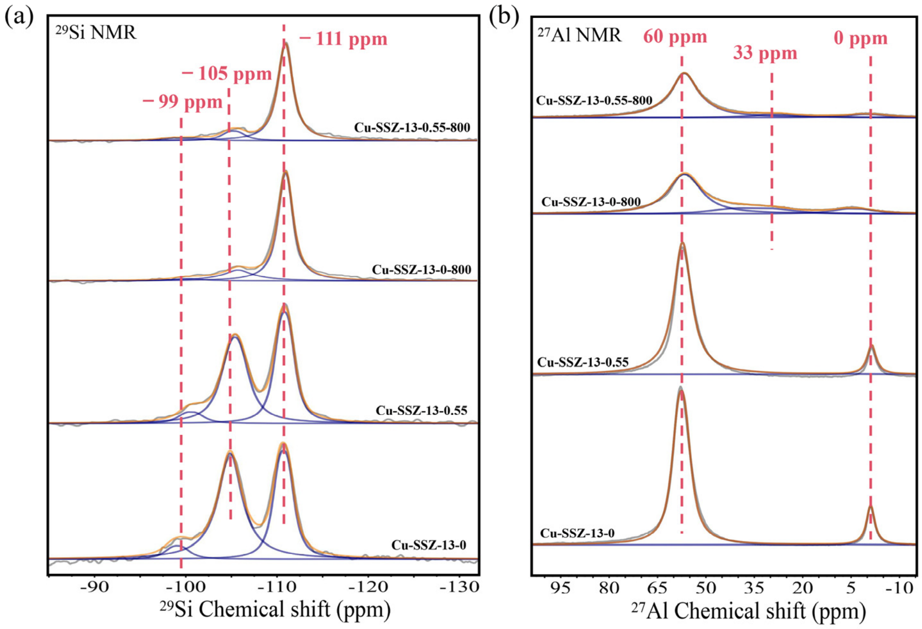

Figure 8. (**a**) ^{29}Si MAS NMR and (**b**) ^{27}Al MAS NMR spectra with curve fittings of Cu-SSZ-13-0 and Cu-SSZ-13-0.55 catalysts before and after hydrothermal aging.

Table 3. ^{29}Si MAS NMR spectra deconvolution results.

Sample	**Si/Al Ratio** [a]	**Proportion of Q^4(nAl) (%)**		
		Q^4(0Al)	**Q^4(1Al)**	**Q^4(2Al)**
Cu-SSZ-13-0	5.9	38	56	6
Cu-SSZ-13-0.55	6.5	77	19	4
Cu-SSZ-13-0-800	15.2	44	50	6
Cu-SSZ-13-0.55-800	16.5	78	20	2

[a] Determined by ^{29}Si MAS NMR spectra.

^{27}Al MAS NMR spectra of the fresh catalysts display two features at 60 and 0 ppm, corresponding to the tetra-coordinated framework Al and hexa-coordinated extra-framework Al, respectively [39–41]. After hydrothermal aging, the feature at 33 ppm arising from the penta-coordinated extra-framework Al emerged, which was strong evidence of Al ions detaching from the framework [42]. Similarly, the proportions of different Al species are also estimated by the deconvolution of ^{27}Al MAS NMR spectra, and the results are listed in Table 4. The proportion of extra-framework Al sites (including penta-coordinated Al and hexa-coordinated Al) of Cu-SSZ-13-0.55 is smaller than that of Cu-SSZ-13-0 after hydrothermal aging. Notably, this difference becomes particularly pronounced after hydrothermal aging, indicating the introduction of mesopores in microporous zeolite effectively inhibits its dealumination from the zeolite framework. These results also proved that the zeolite framework of hierarchically porous Cu-SSZ-13-0.55 is more stable than that of microporous counterpart.

Table 4. ^{27}Al MAS NMR spectra deconvolution results.

Sample	Tera-Coordinated Al (%)	Penta-Coordinated Al (%)	Hexa-Coordinated Al (%)
Cu-SSZ-13-0	88	0	12
Cu-SSZ-13-0.55	90	0	10
Cu-SSZ-13-0-800	71	18	11
Cu-SSZ-13-0.55-800	83	9	8

Since the Cu ions are known as active sites in the NH_3-SCR reaction, the X-ray photoelectron spectroscopy (XPS) was employed to clarify and quantify the Cu species in Cu-SSZ-13-0.55 and Cu-SSZ-13-0. The Cu $2p_{3/2}$ peaks are detected in the ranges of 932.0–938.0 eV (Figure 9a), and the peak around 940.0–948.0 eV is a fingerprint signal indicative of the Cu^{2+} species. The Cu $2p_{3/2}$ peak can be deconvoluted into two peaks at 935.7 and 933.0 eV, which are attributed to Cu^{2+} and CuO_x species [43–45]. The XPS spectrum of Cu-SSZ-13-0.55 catalyst is similar to that of Cu-SSZ-13-0, and an analogous phenomenon is observed in the hydrothermal aging samples. Furthermore, the peak of Cu^{2+} species shifts toward a higher binding energy after hydrothermal aging, which could be ascribed to the charge transfer of Cu ions to the zeolite matrix; consequently, a stronger interaction occurs between Cu ions and zeolites [46]. Moreover, the peak intensities of CuO_x species in the hydrothermally aged catalysts increase, while those of Cu^{2+} species decrease, indicating a low Cu^{2+} concentration owing to the agglomeration of CuO_x species. Figure 9b summarizes the quantitative results of XPS spectra. Cu-SSZ-13-0.55 possesses a higher proportion of Cu^{2+} than that of Cu-SSZ-13-0, being conducive to improving the low-temperature activity. After hydrothermal aging, the proportion of CuO_x increases as the aggregation of CuO_x species on the surface. Notably, Cu-SSZ-13-0.55-800 maintain a lower proportion of CuO_x, suggesting that the introduction of mesopores effectively inhibits the transformation from Cu^{2+} to CuO_x, thus maintaining the good SCR activity.

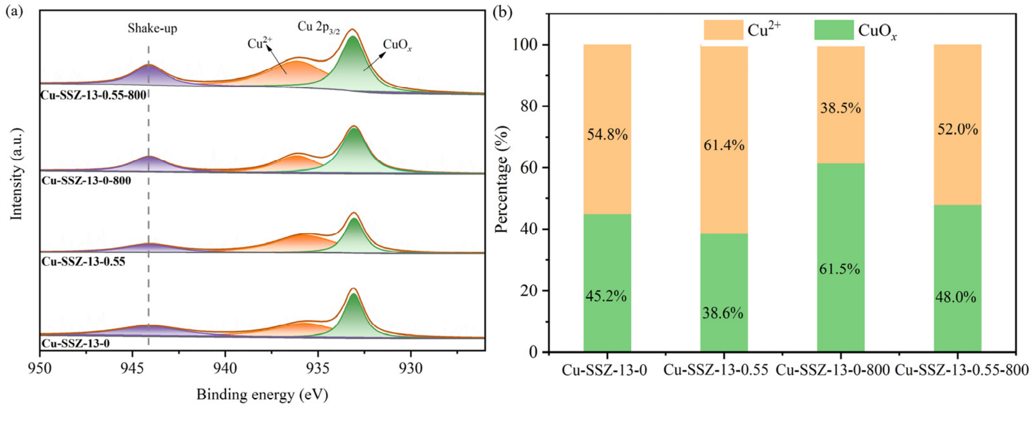

Figure 9. (**a**) Cu 2p XPS spectra and (**b**) quantitative data of Cu species for Cu-SSZ-13-0 and Cu-SSZ-13-0.55 catalysts before and after hydrothermal aging.

2.4. Redox Property and Acidity of Cu-SSZ-13-x Catalysts

To further elucidate the status of Cu species in the catalysts, the temperature programmed reduction of hydrogen (H_2-TPR) was carried out from 50 to 700 °C, and the results are shown in Figure 10a. According to the literature, three different Cu species probably exist in Cu-based zeolites, including $[Cu(OH)]^+$ ions located in the window of eight-membered rings balanced with one framework negative charge (denoted as ZCuOH), Cu^{2+} ions located in the window of six-membered rings and balanced with two framework negative charges (denoted as Z_2Cu), and CuO_x [36]. Actually, the whole H_2 reduction curve can be divided into four distinct peaks. The peak at around 250 °C is ascribed to the reduction of ZCuOH to Cu^+ at the 8MR, while the peak at around 300 °C is attributed to the reduction of CuO_x to Cu^0 [42,45]. In addition, the shoulder peak at around 350 °C is ascribed to the reduction of Z_2Cu to Cu^+ at the 6MR, which requires a higher reduction temperature compared to ZCuOH, due to its higher stability in the CHA structure. The high-temperature peak at 510 °C corresponds to the reduction of Cu^+ to Cu^0 [42,47,48]. In comparison with Cu-SSZ-13-0, the reduction peaks of Cu-SSZ-13-0.55 in the low-temperature region (<350 °C) shift to lower temperatures, while the reduction peaks in the high-temperature region (≥350 °C) shift about 50 °C higher. These results reveal that the improved redox performance of ZCuOH and CuO_x species and the enhanced interactions between Z_2Cu and zeolites are conducive to the low-temperature SCR activity and hydrothermal stability of Cu-SSZ-13-0.55 [36,45,48,49].

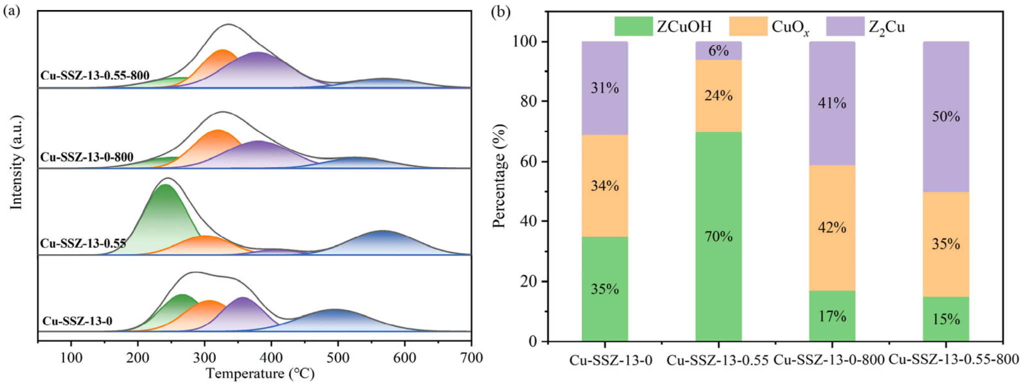

Figure 10. (**a**) H_2-TPR curves and (**b**) quantitative data of Cu species for Cu-SSZ-13-0 and Cu-SSZ-13-0.55 catalysts before and after hydrothermal aging.

The H_2 consumption of the reduction peaks is calibrated to CuO as a standard, and the fractions of different Cu species are calculated by integrating the reduction peaks (Figure 10b). Theoretically, the H_2 consumption of reduction from Cu^+ to Cu^0 should be equal to the sum of those of the first and the third reduction peaks. However, this is not the case in our results. Actually, some of the Cu^+ species located in much more stable sites cannot be reduced at temperatures lower than 900 °C because of the strong interaction between Cu ions and zeolitic frameworks [50]. As shown in Figure 10b, the fraction of ZCuOH in Cu-SSZ-13-0.55 is much higher than that in Cu-SSZ-13-0 while the fractions of CuO_x and Z_2Cu species are lower, contributing to higher low-temperature activity of Cu-SSZ-13-0.55 (Figure 5a). After hydrothermal treatment, nearly one half of ZCuOH sites in Cu-SSZ-13-0 converted to more stable Z_2Cu sites, while the other transformed into CuO_x. In the case of Cu-SSZ-13-0.55, most ZCuOH sites transformed into Z_2Cu sites, and the rest of the ZCuOH sites agglomerated into CuO_x. In summary, Cu-SSZ-13-0.55-800 possesses more Cu^{2+} species (ZCuOH + Z_2Cu) and less CuO_x species in comparison with Cu-SSZ-13-0-800, which is consistent with XPS results (Figure 9b). These results guarantee better SCR activity as well as the hydrothermal stability of Cu-SSZ-13-0.55-800 (Figure 5).

Besides the redox property, the acidity is another determining factor for the catalytic performance of SCR catalysts [51]. Therefore, the temperature-programmed desorption of ammonia (NH_3-TPD) experiments were performed to measure the acidity of the catalysts. In order to better clarify the attribution of acid sites, NH_3-TPD curves of SSZ-13 zeolites in protonic form (H-SSZ-13-*x*) were firstly measured (Figure S5 and Table S1). Two peaks of NH_3 desorption located at 150 and 450 °C are attributed to loosely bonded NH_3 on terminal hydroxyls (i.e., Al-OH and Si-OH) with weak acidity (peak α) and NH_3 adsorbed on Si-O(H)-Al sites with strong acidity (peak γ), respectively [52–54]. Accordingly, the desorption of NH_3 occurs only on the Brønsted acid sites in H-SSZ-13 zeolites. The total amount of NH_3 desorbed from H-SSZ-13-0.55 is slightly higher than that of H-SSZ-13-0 (Table S1); meanwhile, H-SSZ-13-0.55 possesses more weak acid sites as the more terminally hydroxyl species generated by introducing mesopores in the microporous zeolite. As shown in Figure 11, a new NH_3 desorption peak is observed in NH_3-TPD curves of Cu-SSZ-13-*x* catalysts apart from the two peaks. Peak β at around 250 °C corresponds to the NH_3 adsorbed on the strong Lewis acid sites that derive from the isolated Cu^{2+} ions [39,42,45,55]. Consequently, the isolated Cu^{2+} ions not only act as redox sites but also provide Lewis acid sites, delivering excellent SCR activity of Cu-based zeolite catalysts. Cu-SSZ-13-0 and Cu-SSZ-13-0.55 exhibit almost the same NH_3-TPD curves, indicating that they possess comparable acid density and strength at both weak and strong acid sites [39]. However, the acidity changes a lot after hydrothermal aging, and the intensity of peak α and γ significantly decrease. The decrease in peak α can be attributed to the loss of physically adsorbed sites or surface hydroxyl groups, while for peak γ, the reduction is caused by the skeleton collapse of zeolite and the loss of active Cu^{2+} ions [56–60]. Differently, the intensity of peak β increases, indicating that the additional Lewis acid sites arise from transformation of metastable ZCuOH to more stable Z_2Cu and highly dispersed CuO_x during hydrothermal aging [55,61], which is inconsistent with H_2-TPR results (Figure 10). Overall, Cu-SSZ-13-0.55 only lost 33.9% acid sites after hydrothermal aging; however, Cu-SSZ-13-0 has a value of 45.7%. The less disruptive effect to acid sites of Cu-SSZ-13-0.55 is related to its higher content of Z_2Cu^{2+}, which derives from the introduction of mesopores in the Cu-SSZ-13 catalyst.

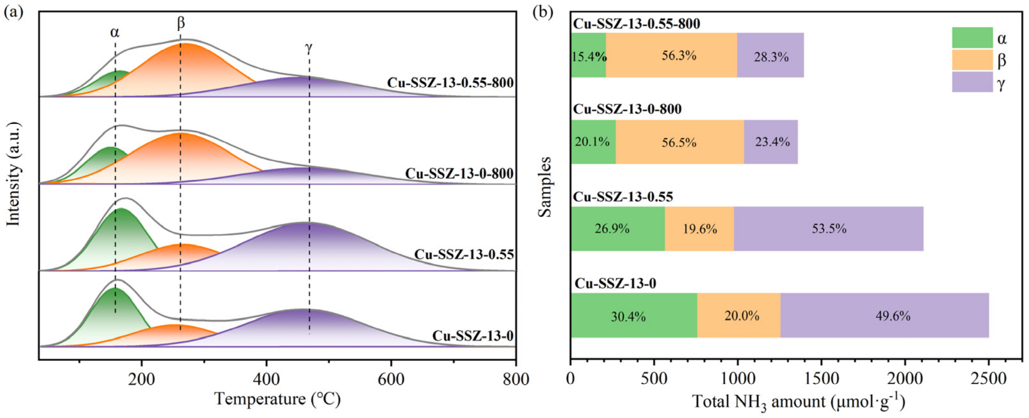

Figure 11. (**a**) NH_3-TPD curves and (**b**) quantitative data of acid sites for Cu-SSZ-13-0 and Cu-SSZ-13-0.55 catalysts before and after hydrothermal aging.

2.5. Reaction Kinetics of Cu-SSZ-13-x Catalysts

The kinetic tests were performed at a high GHSV to exclude external diffusion limitation and at low conversion (<15%) to eliminate internal diffusion limitation. The apparent activation energy (E_a) was estimated using the data obtained in the temperature range (130–180 °C) (Figure 12 and Table S2). The E_a values of Cu-SSZ-13-0 and Cu-SSZ-13-0.55 are 33.4 and 36.3 $kJ \cdot mol^{-1}$ (Figure 12a), respectively, indicating the identical catalytic centers and reaction mechanism [42,62,63]. Combined with the SCR performance of the two catalysts, the promoted low-temperature activity of Cu-SSZ-13-0.55 is due to the reduced diffusion limitation by introducing mesopores in microporous Cu-SSZ-13 catalyst. After hydrothermal aging, the reaction rates of catalysts decrease (Table S2); accordingly, the E_a values of Cu-SSZ-13-0.55-800 and Cu-SSZ-13-0-800 increase to 40.2 and 46.3 $kJ \cdot mol^{-1}$, respectively (Figure 12b). Coincidentally, the low-temperature SCR activity of Cu-SSZ-13-0.55-800 is higher than that of Cu-SSZ-13-0-800, correlating well with its lower activation barrier [42,64]. These results are in accordance with our previous hypothesis, in which the hierarchically porous Cu-SSZ-13 catalysts would exhibit an improved NH_3-SCR performance due to its ability to shorten the diffusion path of reactants/products, thus reducing intra-particle diffusion limitations.

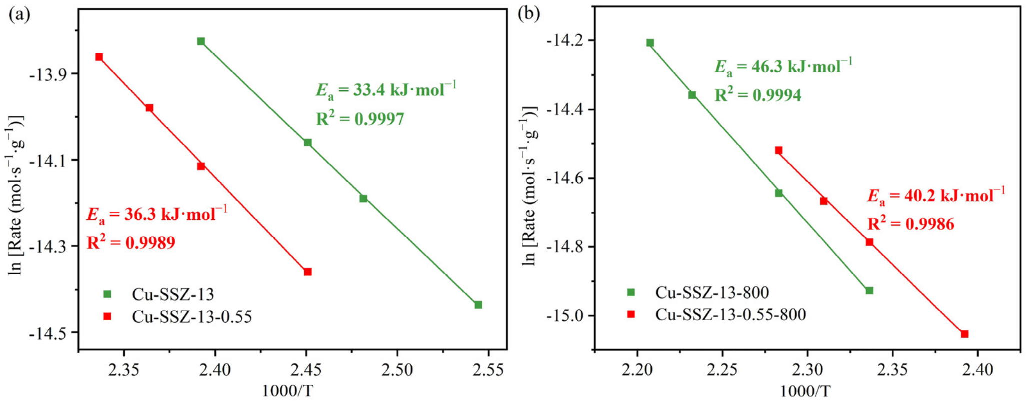

Figure 12. Arrhenius plots of Cu-SSZ-13-0 and Cu-SSZ-13-0.55 catalysts (**a**) before and (**b**) after hydrothermal aging.

3. Materials and Methods

3.1. Preparation

The hierarchically porous SSZ-13 zeolite was synthesized via a trans-crystallization of an FAU zeolite with carbon black as a hard template. Typically, sodium hydroxide (NaOH, 0.83 g, Sinopharm Chemical Reagent Co., Ltd., Beijing, China) was dissolved in deionized water (H_2O, 40.84 g), and then a certain amount of carbon black (CB, Cabot Corporation, Boston, MA, USA) was added into the above solution under ultrasonic treatment until forming a uniform suspension. Thereafter, TMAdaOH (6.6 mL, Sachem Wuxi Co., Ltd., Wuxi, China) was added to the mixture under stirring at room temperature for 30 min. Subsequently, sodium silicate (Na_2SiO_3, 11.1 mL, Merck KGaA, Darmstadt, Germany) and H-type FAU zeolite (Y zeolite, Si/Al = 3.1, 2.0 g, Nankai University Catalyst Co., Ltd., Tianjin, China) were added and vigorously stirred for 1 h, and the final molar composition of the mixture was as follows: 1 SiO_2: 0.041 Al_2O_3: 0.37 NaOH: 0.087 SDA: x CB: 29 H_2O. The mixture was transferred to a Teflon-lined stainless-steel autoclave (100 mL, Yantai Songling Chemical Equipment Co., Ltd., Yantai, China) and further crystallized at 140 °C for 24 h. The as-prepared zeolite was obtained by centrifugation, washing, and drying at 105 °C overnight. Finally, to remove SDA and CB, SSZ-13-x zeolites were obtained by calcination at 575 °C for 8 h in air, where "x" represents the molar composition of CB in the initial mixture before crystallization (x = 0, 0.33, 0.55, 0.77).

The hierarchically porous Cu-SSZ-13-x catalysts were prepared via an ion-exchange method. Firstly, SSZ-13-x zeolite was ion-exchanged with an excess amount of $(NH_4)_2SO_4$ solution (0.33 mol·L^{-1}, 46 mL, Sinopharm Chemical Reagent Co., Ltd., Beijing, China) at 80 °C for 2 h to obtain its NH_4^+ form. And then, the solid was filtered and dried at 105 °C overnight, and mixed with a $CuSO_4$ solution (0.1 mol·L^{-1}, 80 mL, Sinopharm Chemical Reagent Co., Ltd., Beijing, China) under stirring at 80 °C for 1 h. The obtained suspension was centrifuged and thoroughly washed with deionized water. After drying at 105 °C overnight and calcinating at 575 °C for 8 h, Cu-SSZ-13-x catalysts were obtained. The H-SSZ-13-x were prepared via calcinating NH_4-SSZ-13-x at 575 °C for 4 h in air. Hydrothermal aging of Cu-SSZ-13-x catalysts was carried out in a flowing wet-air stream containing 10 vol.% H_2O and held at 800 °C for 16 h. The obtained aged catalysts were denoted as Cu-SSZ-13-x-800.

3.2. Characterizations

Powder X-ray diffraction (XRD) patterns were collected on a Bruker D8 Focus diffractometer (Bruker, Saarbrucken, Germany) using a Cu Kα radiation over a 2θ range from 5° to 50° with a step length of 0.02°. The surface area and porosity were determined by N_2 adsorption/desorption measurements on a Micromeritics ASAP 2020M instrument (Micromeritics, Norcross, GA, USA). The scanning electron microscope (SEM) equipped with energy dispersive spectroscopy (EDS) was performed on a GeminiSEM 300 microscope

(Carl Zeiss, Oberkochen, Germany). Magnetic angle spinning nuclear magnetic resonance (MAS NMR) experiments were conducted on a Bruker AVANCE NEO 600 WB (Bruker, Saarbrucken, Germany). The resonance frequencies of ^{29}Si and ^{27}Al were 119.23 and 156.38 MHz, respectively. A 4 mm MAS probe at a spinning frequency of 10 kHz, recycle delay of 2 s, and a $\pi/2$ pulse length of 1.67 µs were applied on the recording of ^{29}Si MAS NMR spectra. A 4 mm MAS probe at a spinning frequency of 15 kHz, 20 s pulse delay, and a $\pi/2$ pulse length of 1.67 µs was utilized to record ^{27}Al MAS NMR spectra. X-ray photoelectron spectroscopy (XPS) was performed on an AXIS Supra instrument (Shimadzu, Kyoto, Japan), and the binding energies were calibrated using the C 1 s peak at 284.8 eV. The temperature-programmed reduction of hydrogen (H_2-TPR) experiments were performed on a XIANQUAN TP-5080D chemisorption analyzer (XIANQUAN, Tianjin, China) equipped with a thermal conductivity detector (TCD). The temperature-programmed desorption of ammonia (NH_3-TPD) experiments were conducted in a quartz reactor using quadrupole mass spectrometer (OmniStar GSD 320, Pfeiffer, Germany) to monitor NH_3. Prior to the experiments, a 50 mg sample was pretreated at 400 °C for 0.5 h in 10 vol.% O_2/He and cooled to 30 °C. NH_3 adsorption was operated in 0.4 vol.% NH_3/He until saturation. Then, the samples were pretreated with He to purify the surface. Finally, the samples were heated from room temperature to 800 °C with a ramp rate of 10 $°C \cdot min^{-1}$.

3.3. Catalyst Activity and Reaction Kinetics Measurements

The NH_3-SCR activity was tested in a fixed-bed quartz tube reactor (6.0 mm i.d.) with a thermocouple placed inside the catalyst bed in the temperature range of 150–600 °C. The model flue gas consisted of 500 ppm NO, 500 ppm NH_3, 5.3 vol.% O_2, and balanced He. The powder samples were pressed, crushed, and sieved into 40–60 mesh prior to use. The volume of catalyst was 0.09 mL (or 0.045 mL), and the total flow rate was kept at 600 $mL \cdot min^{-1}$ corresponding to a gas hourly space velocity (GHSV) of 400,000 h^{-1} (or 800,000 h^{-1}). The chemiluminescence NO_x analyzer (Model 42*i*-HL, Thermo Electron Corporation, Waltham, MA, USA) was used to monitor the concentrations of NO and NO_2, while the quadrupole mass spectrometer (OmniStar 301, Pfeiffer, Germany) was employed for detecting N_2O and NH_3. The data for steady-state activity of the catalysts were collected after about 1 h on stream.

The kinetics tests were performed under similar conditions as the steady-state reaction, whereas the GHSV was estimated to be 800,000 h^{-1} with the amount of catalyst decreased to 0.045 mL (100–200 mesh). The isothermal reactions were conducted at a temperature at which a stable and low conversion of NO_x (<15%) was achieved in an approximate kinetic regime [65].

4. Conclusions

The hierarchically porous SSZ-13 zeolite was synthesized via a trans-crystallization method assisted by using carbon black as a hard template in a short synthetic period. The corresponding catalysts were prepared by Cu ion exchange, and the introduction of mesopores made more active Cu species enter the ion-exchange sites easily and smoothly. Consequently, the as-synthesized hierarchically porous Cu-SSZ-13 catalysts possess higher Cu loadings, thus promoting low-temperature SCR activity compared with their microporous counterpart. In addition, hydrothermal resistance is significantly enhanced, and the SCR activity of hierarchically porous Cu-SSZ-13 catalysts is improved across the whole temperature range. Therefore, the mesopores not only stabilize the zeolite structure but also maintain Cu species in ionic form, which are the active sites of SCR catalysts. Furthermore, the intra-particle diffusion limitations are reduced by mesopores in SSZ-13 zeolites due to the reduction in diffusion path length. The kinetic results demonstrate that introduction of mesopores in Cu-SSZ-13 catalysts could accelerate the reaction rate and lower the activation energy of NH_3-SCR reaction, implying that mass transportation plays a crucial role in eliminating NO_x on such small porous zeolite catalysts. This work provided a new method to synthesize hierarchically porous zeolites and catalysts for more efficient adsorptions and catalytic reactions.

Supplementary Materials: The following supporting information can be downloaded at: https://www.mdpi.com/article/10.3390/catal13081217/s1, Figure S1: N_2 selectivity of (a) Cu-SSZ-13-*x* and (b) Cu-SSZZ-13-*x*-800 catalysts; Figure S2: (a) NO_x conversion and (b) N_2 selectivity of Cu-SSZ-13-*x* catalysts at a gas hourly space velocity of 800,000 h^{-1}; Figure S3: (a) N_2 adsorption/desorption isotherms and (b) pore size distribution curves of Cu-SSZ-13-0 and Cu-SSZ-13-0.55 catalysts before and after hydrothermal aging; Figure S4: Si and Al elements EDS mappings of (a) Cu-SSZ-13-0, (b) Cu-SSZ-13-0.55, (c) Cu-SSZ-13-0-800, and (d) Cu-SSZ-13-0.55-800; Figure S5: NH_3-TPD curves of H-SSZ-13-0 and H-SSZ-13-0.55 zeolites; Table S1: Quantification of NH_3-TPD results for H-SSZ-13-0 and H-SSZ-13-0.55 zeolites; Table S2: Kinetic catalytic performances of Cu-SSZ-13-0 and Cu-SSZ-13-0.55 catalysts before and after hydrothermal aging.

Author Contributions: Conceptualization, Y.X.; formal analysis, F.Y., Y.X., X.Z., L.Y. and D.H.; investigation, F.Y., X.Z., A.T. and L.Y.; data curation, F.Y., X.Z., A.T., D.H., J.J. and Y.L.; writing—original draft preparation, F.Y.; writing—review and editing, Y.X. and Z.Z.; supervision, Y.X. and Z.Z.; funding acquisition, Y.X. and Z.Z. All authors have read and agreed to the published version of the manuscript.

Funding: This research was funded by National Natural Science Foundation of China (No. 22076062 and 22276070), China Postdoctoral Science Foundation (No. 2022M711957), National Engineering Laboratory for Mobile Source Emission Control Technology (No. NELMS2019A14), and Project of Jinan Municipal Bureau of Science and Technology (No. 2020GXRC021).

Data Availability Statement: The data presented in this study are available on request from the corresponding author.

Conflicts of Interest: The authors declare no conflict of interest.

References

1. Wang, J.; Zhao, H.; Haller, G.; Li, Y. Recent advances in the selective catalytic reduction of NO_x with NH_3 on Cu-Chabazite catalysts. *Appl. Catal. B Environ.* **2017**, *202*, 346–354. [CrossRef]
2. Wu, T.; Cui, Y.; Lian, A.; Tian, Y.; Li, R.; Liu, X.; Yan, J.; Xue, Y.; Liu, H.; Wu, B. Vehicle emissions of primary air pollutants from 2009 to 2019 and projection for the 14th Five-Year Plan period in Beijing, China. *J. Environ. Sci.* **2023**, *124*, 513–521. [CrossRef] [PubMed]
3. Xu, G.; Shan, W.; Yu, Y.; Shan, Y.; Wu, X.; Wu, Y.; Zhang, S.; He, L.; Shuai, S.; Pang, H.; et al. Advances in emission control of diesel vehicles in China. *J. Environ. Sci.* **2023**, *123*, 15–29. [CrossRef] [PubMed]
4. Luo, J.; Xu, H.; Liang, X.; Wu, S.; Liu, Z.; Tie, Y.; Li, M.; Yang, D. Research progress on selective catalytic reduction of NO_x by NH_3 over copper zeolite catalysts at low temperature: Reaction mechanism and catalyst deactivation. *Res. Chem. Intermed.* **2022**, *49*, 2321–2357. [CrossRef]
5. Xin, Y.; Li, Q.; Zhang, Z. Zeolitic materials for deNO_x selective catalytic reduction. *ChemCatChem* **2018**, *10*, 29–41. [CrossRef]
6. Kwak, J.; Tonkyn, R.; Kim, D.; Szanyi, J.; Peden, C. Excellent activity and selectivity of Cu-SSZ-13 in the selective catalytic reduction of NO_x with NH_3. *J. Catal.* **2010**, *275*, 187–190. [CrossRef]
7. Qi, X.; Wang, Y.; Liu, C.; Liu, Q. The challenges and comprehensive evolution of Cu-based zeolite catalysts for SCR systems in diesel vehicles: A review. *Catal. Surv. Asia* **2022**. [CrossRef]
8. Xie, L.; Liu, F.; Ren, L.; Shi, X.; Xiao, F.; He, H. Excellent performance of one-pot synthesized Cu-SSZ-13 catalyst for the selective catalytic reduction of NO_x with NH_3. *Environ. Sci. Technol.* **2014**, *48*, 566–572. [CrossRef]
9. Zhao, Z.; Yu, R.; Zhao, R.; Shi, C.; Gies, H.; Xiao, F.; DeVos, D.; Yokoi, T.; Bao, X.; Kolb, U.; et al. Cu-exchanged Al-rich SSZ-13 zeolite from organotemplate-free synthesis as NH_3-SCR catalyst: Effects of Na^+ ions on the activity and hydrothermal stabiliy. *Appl. Catal. B Environ.* **2017**, *217*, 421–428. [CrossRef]
10. Li, P.; Xin, Y.; Zhang, H.; Yang, F.; Tang, A.; Han, D.; Jia, J.; Wang, J.; Li, Z.; Zhang, Z. Recent progress in performance optimization of Cu-SSZ-13 catalyst for selective catalytic reduction of NO_x. *Front. Chem.* **2022**, *10*, 1033255. [CrossRef]
11. Deka, U.; Lezcano-Gonzalez, I.; Weckhuysen, B.; Beale, A. Local environment and nature of Cu active sites in zeolite-based catalysts for the selective catalytic reduction of NO_x. *ACS Catal.* **2013**, *3*, 413–427. [CrossRef]
12. Liu, C.; Bi, Y.; Han, J.; Guo, M.; Liu, Q. A Perspective on the relationship between microstructure and performance of Cu-based zeolites for the selective catalytic reduction of NO_x. *Catal. Surv. Asia* **2020**, *24*, 179–195. [CrossRef]
13. Gao, F.; Walter, E.; Karp, E.; Luo, J.; Tonkyn, R.; Kwak, J.; Szanyi, J.; Peden, C. Structure-activity relationships in NH_3-SCR over Cu-SSZ-13 as probed by reaction kinetics and EPR studies. *J. Catal.* **2013**, *300*, 20–29. [CrossRef]

14. Kumar, M.; Luo, H.; Roman-Leshkov, Y.; Rimer, J. SSZ-13 crystallization by particle attachment and deterministic pathways to crystal size control. *J. Am. Chem. Soc.* **2015**, *137*, 13007–13017. [CrossRef] [PubMed]
15. Liu, B.; Zhao, X.; Mao, W.; Chen, H.; Han, L.; Zhu, K.; Zhou, X. Pickering emulsion mediated crystallization of hierarchical zeolite SSZ-13 with enhanced NH_3 selective catalytic reduction performance. *Microporous Mesoporous Mater.* **2019**, *285*, 202–214. [CrossRef]
16. Koohsaryan, E.; Anbia, M. Nanosized and hierarchical zeolites: A short review. *Chin. J. Catal.* **2016**, *37*, 447–467. [CrossRef]
17. Chen, L.; Sun, M.; Wang, Z.; Yang, W.; Xie, Z.; Su, B. Hierarchically structured zeolites: From Design to application. *Chem. Rev.* **2020**, *120*, 11194–11294. [CrossRef]
18. Liu, Z.; Hua, Y.; Wang, J.; Dong, X.; Tian, Q.; Han, Y. Recent progress in the direct synthesis of hierarchical zeolites: Synthetic strategies and characterization methods. *Mater. Chem. Front.* **2017**, *1*, 2195–2212. [CrossRef]
19. Chen, L.; Li, X.; Rooke, J.C.; Zhang, Y.; Yang, X.; Tang, Y.; Xiao, F.; Su, B. Hierarchically structured zeolites: Synthesis, mass transport properties and applications. *J. Mater. Chem.* **2012**, *22*, 17381–17403. [CrossRef]
20. Zhang, L.; Sun, X.; Pan, M.; Yang, X.; Liu, Y.; Sun, J.; Wan, Q.; Zheng, J.; Wang, Y.; Ma, J.; et al. Interfacial effects between carbon nanotube templates and precursors on fabricating a wall-crystallized hierarchical pore system in zeolite crystals. *J. Mater. Sci.* **2020**, *55*, 10412–10426. [CrossRef]
21. Wang, H.; Du, G.; Jia, J.; Chen, S.; Su, Z.; Chen, R.; Chen, T. Hierarchically porous zeolites synthesized with carbon materials as templates. *Front. Chem. Sci. Eng.* **2021**, *15*, 1444–1461. [CrossRef]
22. Wu, L.; Degirmenci, V.; Magusin, P.; Szyja, B.; Hensen, E. Dual template synthesis of a highly mesoporous SSZ-13 zeolite with improved stability in the methanol-to-olefins reaction. *Chem. Commun.* **2012**, *48*, 9492–9494. [CrossRef] [PubMed]
23. Zhu, X.; Rohling, R.; Filonenko, G.; Mezari, B.; Hofmann, J.; Asahina, S.; Hensen, E. Synthesis of hierarchical zeolites using an inexpensive mono-quaternary ammonium surfactant as mesoporogen. *Chem. Commun.* **2014**, *50*, 14658–14661. [CrossRef]
24. Liu, L.; Chen, Z.; Qu, H.; Yuan, J.; Yu, M.; Xie, H.; Zhong, Q. Dual-template assembled hierarchical Cu-SSZ-13: Morphology evolution, crystal growth and stable high-temperature selective catalytic reduction performance. *CrystEngComm* **2020**, *22*, 7036–7045. [CrossRef]
25. Peng, C.; Yan, R.; Mi, Y.; Li, G.; Zheng, Y.; Luo, Y.; Liang, J.; Liu, W.; Li, Z.; Wu, D.; et al. Toward rational design of a novel hierarchical porous Cu-SSZ-13 catalyst with boosted low-temperature NO reduction performance. *J. Catal.* **2021**, *401*, 309–320. [CrossRef]
26. Serrano, D.; Escola, J.; Pizarro, P. Synthesis strategies in the search for hierarchical zeolites. *Chem. Soc. Rev.* **2013**, *42*, 4004–4035. [CrossRef] [PubMed]
27. Bai, R.; Song, Y.; Li, Y. Creating hierarchical pores in zeolite catalysts. *Trends Chem.* **2019**, *1*, 601–611. [CrossRef]
28. Liang, J.; Tao, J.; Mi, Y.; Liu, W.; Wang, Z.; Li, Z.; Wu, D.; Wu, P.; Peng, H. Unraveling the boosting low-temperature performance of ordered mesoporous Cu-SSZ-13 catalyst for NO_x reduction. *Chem. Eng. J.* **2021**, *409*, 128238. [CrossRef]
29. Li, D.; Chen, Y.; Hu, J.; Deng, B.; Cheng, X.; Zhang, Y. Synthesis of hierarchical chabazite zeolite via interzeolite transformation of coke-containing spent MFI. *Appl. Catal. B Environ.* **2020**, *270*, 118881. [CrossRef]
30. Itakura, M.; Goto, I.; Takahashi, A.; Fujitani, T.; Ide, Y.; Sadakane, M.; Sano, T. Synthesis of high-silica CHA type zeolite by interzeolite conversion of FAU type zeolite in the presence of seed crystals. *Microporous Mesoporous Mater.* **2011**, *144*, 91–96. [CrossRef]
31. Liang, J.; Mi, Y.; Song, G.; Peng, H.; Li, Y.; Yan, R.; Liu, W.; Wang, Z.; Wu, P.; Liu, F. Environmental benign synthesis of nano-SSZ-13 via FAU trans-crystallization: Enhanced NH_3-SCR performance on Cu-SSZ-13 with nano-size effect. *J. Hazard. Mater.* **2020**, *398*, 122986. [CrossRef] [PubMed]
32. Zhang, T.; Chang, H.; You, Y.; Shi, C.; Li, J. Excellent activity and selectivity of one-pot synthesized Cu-SSZ-13 catalyst in the selective catalytic oxidation of ammonia to nitrogen. *Environ. Sci. Technol.* **2018**, *52*, 4802–4808. [CrossRef]
33. Zhang, N.; Xin, Y.; Li, Q.; Ma, X.; Qi, Y.; Zheng, L.; Zhang, Z. Ion exchange of one-pot synthesized Cu-SAPO-44 with NH_4NO_3 to promote Cu dispersion and activity for selective catalytic reduction of NO_x with NH_3. *Catalysts* **2019**, *9*, 882. [CrossRef]
34. Zhang, T.; Qiu, F.; Li, J. Design and synthesis of core-shell structured meso-Cu-SSZ-13@mesoporous aluminosilicate catalyst for SCR of NO with NH_3: Enhancement of activity, hydrothermal stability and propene poisoning resistance. *Appl. Catal. B Environ.* **2016**, *195*, 48–58. [CrossRef]
35. Sunil Kumar, S.; Alphin, M.S.; Senthil Kumar, P.; Raja, S. A review on zeolite catalyst for deNO_x performance in ammonia-selective catalytic reduction. *Fuel* **2023**, *334*, 126828. [CrossRef]
36. Song, J.; Wang, Y.; Walter, E.; Washton, N.; Mei, D.; Kovarik, L.; Engelhard, M.; Prodinger, S.; Wang, Y.; Peden, C.; et al. Toward rational design of Cu/SSZ-13 selective catalytic reduction catalysts: Implications from atomic-level understanding of hydrothermal stability. *ACS Catal.* **2017**, *7*, 8214–8227. [CrossRef]
37. Xiong, W.; Liu, L.; Guo, A.; Chen, D.; Shan, Y.; Fu, M.; Wu, J.; Ye, D.; Chen, P. Economical and sustainable synthesis of small-pore chabazite catalysts for NO_x abatement by recycling organic structure-directing agents. *Environ. Sci. Technol.* **2023**, *57*, 655–665. [CrossRef]
38. Dědeček, J.; Sklenak, S.; Li, C.; Gao, F.; Brus, J.; Zhu, Q.; Tatsumi, T. Effect of Al/Si substitutions and silanol nests on the local geometry of Si and Al framework sites in silicone-rich zeolites: A combined high resolution ^{27}Al and ^{29}Si NMR and density functional theory/molecular mechanics study. *J. Phys. Chem. C* **2009**, *113*, 14454–14466. [CrossRef]

39. Wang, Y.; Shi, X.; Shan, Y.; Du, J.; Liu, K.; He, H. Hydrothermal stability enhancement of Al-rich Cu-SSZ-13 for NH_3 selective catalytic reduction reaction by ion exchange with cerium and samarium. *Ind. Eng. Chem. Res.* **2020**, *59*, 6416–6423. [CrossRef]
40. Prodinger, S.; Derewinski, M.; Wang, Y.; Washton, N.; Walter, E.; Szanyi, J.; Gao, F.; Wang, Y.; Peden, C. Sub-micron Cu/SSZ-13: Synthesis and application as selective catalytic reduction (SCR) catalysts. *Appl. Catal. B Environ.* **2017**, *201*, 461–469. [CrossRef]
41. Di Iorio, J.; Li, S.; Jones, C.; Nimlos, C.; Wang, Y.; Kunkes, E.; Vattipalli, V.; Prasad, S.; Moini, A.; Schneider, W.; et al. Cooperative and competitive occlusion of organic and inorganic structure-directing agents within chabazite zeolites influences their aluminum arrangement. *J. Am. Chem. Soc.* **2020**, *142*, 4807–4819. [CrossRef] [PubMed]
42. Chen, M.; Li, J.; Xue, W.; Wang, S.; Han, J.; Wei, Y.; Mei, D.; Li, Y.; Yu, J. Unveiling secondary-ion-promoted catalytic properties of Cu-SSZ-13 zeolites for selective catalytic reduction of NO_x. *J. Am. Chem. Soc.* **2022**, *144*, 12816–12824. [CrossRef] [PubMed]
43. Wang, J.; Peng, Z.; Chen, Y.; Bao, W.; Chang, L.; Feng, G. *In-situ* hydrothermal synthesis of Cu-SSZ-13/cordierite for the catalytic removal of NO_x from diesel vehicles by NH_3. *Chem. Eng. J.* **2015**, *263*, 9–19. [CrossRef]
44. Wan, J.; Chen, J.; Zhao, R. One-pot synthesis of Fe/Cu-SSZ-13 catalyst and its highly efficient performance for the selective catalytic reduction of nitrogen oxide with ammonia. *J. Environ. Sci.* **2021**, *100*, 306–316. [CrossRef] [PubMed]
45. Chen, M.; Zhao, W.; Wei, Y.; Han, J.; Li, J.; Sun, C.; Mei, D.; Yu, J. La ions-enhanced NH_3-SCR performance over Cu-SSZ-13 catalysts. *Nano Res.* **2023**. [CrossRef]
46. Xu, R.; Wang, Z.; Liu, N.; Dai, C.; Zhang, J.; Chen, B. Understanding Zn functions on hydrothermal stability in a one-pot-synthesized Cu&Zn-SSZ-13 catalyst for NH_3 selective catalytic reduction. *ACS Catal.* **2020**, *10*, 6197–6212.
47. Kim, Y.; Lee, J.; Min, K.; Hong, S.; Nam, I.; Cho, B. Hydrothermal stability of CuSSZ13 for reducing NO_x by NH_3. *J. Catal.* **2014**, *311*, 447–457. [CrossRef]
48. Chen, J.; Zhao, R.; Zhou, R. A new insight into active Cu^{2+} species properties in one-pot synthesized Cu-SSZ-13 catalysts for NO_x reduction by NH_3. *ChemCatChem* **2018**, *10*, 5182–5189. [CrossRef]
49. Gao, F.; Szanyi, J. On the hydrothermal stability of Cu/SSZ-13 SCR catalysts. *Appl. Catal. A Gen.* **2018**, *560*, 185–194. [CrossRef]
50. Du, J.; Shan, Y.; Sun, Y.; Gao, M.; Liu, Z.; Shi, Y.; Yu, Y.; He, H. Unexpected increase in low-temperature NH_3-SCR catalytic activity over Cu-SSZ-39 after hydrothermal aging. *Appl. Catal. B Environ.* **2021**, *294*, 120237. [CrossRef]
51. Tan, W.; Wang, C.; Yu, S.; Li, Y.; Xie, S.; Gao, F.; Dong, L.; Liu, F. Revealing the effect of paired redox-acid sites on metal oxide catalysts for efficient NO_x removal by NH_3-SCR. *J. Hazard. Mater.* **2021**, *416*, 125826. [CrossRef] [PubMed]
52. Ma, L.; Cheng, Y.; Cavataio, G.; McCabe, R.; Fu, L. In situ DRIFTS and temperature-programmed technology study on NH_3-SCR of NO over Cu-SSZ-13 and Cu-SAPO-34 catalysts. *Appl. Catal. B Environ.* **2014**, *156–157*, 428–437. [CrossRef]
53. Wang, D.; Gao, F.; Peden, C.; Li, J.; Kamasamudram, K.; Epling, W. Selective catalytic reduction of NO_x with NH_3 over a Cu-SSZ-13 catalyst prepared by a solid-state ion-exchange method. *ChemCatChem* **2014**, *6*, 1579–1583. [CrossRef]
54. Gao, F.; Wang, Y.; Washton, N.; Kollár, M.; Szanyi, J.; Peden, C. Effects of alkali and alkaline earth cocations on the activity and hydrothermal stability of Cu/SSZ-13 NH_3-SCR Catalysts. *ACS Catal.* **2015**, *5*, 6780–6791. [CrossRef]
55. Ma, Y.; Wu, X.; Cheng, S.; Cao, L.; Liu, L.; Xu, Y.; Liu, J.; Ran, R.; Si, Z.; Weng, D. Relationships between copper speciation and Brønsted acidity evolution over Cu-SSZ-13 during hydrothermal aging. *Appl. Catal. A Gen.* **2020**, *602*, 117650. [CrossRef]
56. Jiang, H.; Guan, B.; Lin, H.; Huang, Z. Cu/SSZ-13 zeolites prepared by in situ hydrothermal synthesis method as NH_3-SCR catalysts: Influence of the Si/Al ratio on the activity and hydrothermal properties. *Fuel* **2019**, *255*, 115587. [CrossRef]
57. Wang, J.; Fan, D.; Yu, T.; Wang, J.; Hao, T.; Hu, X.; Shen, M.; Li, W. Improvement of low-temperature hydrothermal stability of Cu/SAPO-34 catalysts by Cu^{2+} species. *J. Catal.* **2015**, *322*, 84–90. [CrossRef]
58. Han, S.; Ye, Q.; Cheng, S.; Kang, T.; Dai, H. Effect of the hydrothermal aging temperature and Cu/Al ratio on the hydrothermal stability of CuSSZ-13 catalysts for NH_3-SCR. *Catal. Sci. Technol.* **2017**, *7*, 703–717. [CrossRef]
59. Deng, D.; Deng, S.; He, D.; Wang, Z.; Chen, Z.; Ji, Y.; Yan, G.; Hou, G.; Li, L.; He, H. A comparative study of hydrothermal aging effect on cerium and lanthanum doped Cu/SSZ-13 catalysts for NH_3-SCR. *J. Rare Earths* **2021**, *39*, 969–978. [CrossRef]
60. Gao, Q.; Ye, Q.; Han, S.; Cheng, S.; Kang, T.; Dai, H. Effect of Ce doping on hydrothermal stability of Cu-SAPO-18 in the selective catalytic reduction of NO with NH_3. *Catal. Surv. Asia* **2020**, *24*, 134–142. [CrossRef]
61. Jiang, H.; Guan, B.; Peng, X.; Zhan, R.; Lin, H.; Huang, Z. Influence of synthesis method on catalytic properties and hydrothermal stability of Cu/SSZ-13 for NH_3-SCR reaction. *Chem. Eng. J.* **2020**, *379*, 122358. [CrossRef]
62. Wang, J.; Shao, L.; Wang, C.; Wang, J.; Shen, M.; Li, W. Controllable preparation of various crystal size and nature of intra-crystalline diffusion in Cu/SSZ-13 NH_3-SCR catalysts. *J. Catal.* **2018**, *367*, 221–228. [CrossRef]
63. Zhang, Y.; Peng, Y.; Li, J.; Groden, K.; McEwen, J.; Walter, E.; Chen, Y.; Wang, Y.; Gao, F. Probing active-site relocation in Cu/SSZ-13 SCR catalysts during hydrothermal aging by in situ EPR spectroscopy, kinetics studies, and DFT calculations. *ACS Catal.* **2020**, *10*, 9410–9419. [CrossRef]
64. Fu, Y.; He, G.; Shan, Y.; Du, J. Promotion of the selective catalytic reduction of NO_x with NH_3 over microporous Cu-SSZ-13 by H_2O and OH groups at low temperatures: A density functional theory study. *Catal. Sci. Technol.* **2022**, *12*, 5524–5532. [CrossRef]
65. Xin, Y.; Wang, X.; Li, Q.; Ma, X.; Qi, Y.; Zheng, L.; Anderson, J.; Zhang, Z. The potential of Cu-SAPO-44 in the selective catalytic reduction of NO_x with NH_3. *ChemCatChem* **2016**, *8*, 3740–3745. [CrossRef]